Catalysis Today 169 (2011) 125–137

Contents lists available at ScienceDirect

Catalysis Today

journal homepage: www.elsevier.com/locate/cattod

Partial oxidation of methane on Pt-supported lanthanide doped ceria–zirconia oxides: Effect of the surface/lattice oxygen mobility on catalytic performance

Vladislav A. Sadykov[a,b,*], Nathalia N. Sazonova[a], Aleksei S. Bobin[a,d], Vitalii S. Muzykantov[a], Elena L. Gubanova[a,c], Galina M. Alikina[a], Anton I. Lukashevich[a], Vladimir A. Rogov[a], Eugenia N. Ermakova[b], Ekaterina M. Sadovskaya[a], Nathalia V. Mezentseva[a], Ekaterina G. Zevak[b], Sergei A. Veniaminov[a], Martin Muhler[c], Claude Mirodatos[d], Yves Schuurman[d], Andre C. van Veen[c,d]

[a] Boreskov Institute of Catalysis SB RAS, Pr. Lavrentieva 5, Novosibirsk 630090, Russia
[b] Novosibirsk State University, Pirogova, 2, Novosibirsk 630090, Russia
[c] Lehrstuhl für Technische Chemie, Ruhr-Universität Bochum, Universitätsstraße 150, 44780 Bochum, Germany
[d] Institut de Recherches sur la catalyse et l'environnement de Lyon (IRCELYON), UMR 5256 (CNRS/Université Claude Bernard Lyon1), Université de Lyon – Université Claude Bernard Lyon1, 2 Avenue Albert Einstein, Villeurbanne Cedex 69626, France

ARTICLE INFO

Article history:
Received 19 July 2010
Received in revised form 25 October 2010
Accepted 27 October 2010
Available online 21 December 2010

Keywords:
Selective oxidation of CH_4
Syngas
Pt
Fluorite-like oxides
Oxygen mobility and reactivity
Oxygen isotope exchange
Transient studies
Mechanism

ABSTRACT

Partial oxidation of methane into syngas at short contact times (5–15 ms) was studied in both steady-state and transient modes at temperatures up to 850 °C in realistic feeds (CH_4 content up to 20%, $CH_4/O_2 = 2$) with a minimum impact of mass and heat transfer for structured catalysts carrying $Pt/Ln_{0.3}Ce_{0.35}Zr_{0.35}O_{2-y}$ (Ln = La, Pr, Gd) as thin layers on walls of corundum channel substrates. Oxygen mobility and reactivity of the active phase were characterized by oxygen isotope heteroexchange, temperature-programmed O_2 desorption and CH_4 reduction, isothermal pulse reduction by methane with wide variation of CH_4 concentrations and TAP pulse studies. Experimental data point towards a selective oxidation of methane into syngas via a direct route with oxygen-assisted methane activation. This mechanistic feature is related to the strong Pt-support interaction stabilizing highly dispersed oxidic Pt species less active in CH_4 and syngas combustion than metallic Pt clusters. Support activates O_2 molecules and supplies active oxygen species to Pt sites. A high rate of oxygen diffusion on the surface and in the bulk of the support and Pt-support oxygen spillover stabilizes Pt in a well dispersed partially oxidized state while preventing coking at high concentrations of CH_4 in the feed.

1. Introduction

Detailed studies on the mechanism of catalytic oxidations over oxide catalysts by Prof. Haber combined successfully the point of view of organic and solid state chemists (see, i.e. [1]). He stressed the importance of a reliable estimation of parameters related to the activation and transfer of oxygen on the surface and in the bulk of oxides and their interrelation with the real/defect structure of catalysts changing under the effect of the reaction media. On the other hand, activation and routes of transformation of organic molecules into deep or partial oxidation products strongly depend upon the state of the oxide catalysts surface controlling mobility and reactivity of oxygen species.

Catalytic partial oxidation of methane (CPOM) into syngas at short contact times using monolithic catalysts is now considered as promising alternative to the traditional steam reforming [2]. CPOM presents an interesting (though difficult to study) example of the above mentioned strong interrelation between the catalysts performance characteristics (activity and selectivity of CH_4 transformation into syngas) and surface oxygen mobility and reactivity. Recent research suggests that catalysts comprised of platinum supported on complex fluorite-like oxides Ce–Zr–Ln–O (Ln = Pr, Gd or La) favor the so called direct route of methane oxidation into syngas [3,4]. The direct pathway postulates the formation of H_2 and CO as primary products further oxidized into CO_2 and H_2O depending on process conditions (contact time, O/C ratios, etc.). The main evidence supporting the occurrence of the direct route is the observation of syngas at extremely short contact times in the presence of unreacted oxygen [3]. The question if the reaction mechanism depends on such factors as the mobility/reactivity of the surface/lattice oxygen is still a matter

* Corresponding author at: Boreskov Institute of Catalysis SB RAS, Pr. Lavrentieva 5, Novosibirsk 630090, Russia. Tel.: +7 383 3308763.
E-mail addresses: sadykov@catalysis.ru, vasadykov@mail.ru (V.A. Sadykov).

0920-5861/$ – see front matter © 2010 Elsevier B.V. All rights reserved.
doi:10.1016/j.cattod.2010.10.098

of debates [4]. At least, for Rh supported on α-alumina, which is an example of the oxide with very low (if any) oxygen mobility and reactivity, detailed CPOM studies at realistic feed composition by the group of Forzatti proved that syngas is formed via the indirect combustion-steam reforming route [5]. The latter is due to a faster oxidation of CO and H_2 than that of CH_4 on Rh in the inlet part of reactor where the gas phase oxygen is present. When however small Pt clusters are supported on an oxide with a high lattice oxygen mobility and moderate bonding strength, CH_4 is activated on Pt producing CH_x species while oxygen molecules are activated on the oxide sites. Interaction of CH_x fragments with oxygen species supplied to the Pt-support interface by the surface diffusion (reverse spillover) provides an efficient bifunctional route for the CH_4 transformation into syngas [6,7].

Some arguments in favor of the bifunctional scheme of methane partial oxidation can be obtained by comparing the specific rate of CPOM for catalysts with a comparable Pt dispersion but broadly varying surface/bulk oxygen mobility. This mobility can be estimated by dynamic methods either for the standard oxidized state of samples (oxygen isotope exchange, temperature-programmed oxygen desorption) or for their partially reduced state (H_2 or CH_4 TPR). However, for strengthening the bi-functional scheme, an estimation of the transfer rate of the oxygen-containing species between the Pt particles and the support in the course of catalytic reaction would be of crucial importance. This can be achieved using kinetic transients, where relaxation curves fitting allows to estimate the rate constants of corresponding steps [7–9].

However, papers devoted to the systematic estimation and analysis of the oxygen exchange parameters for a series of Pt-supported doped ceria–zirconia samples are still scarce [10,11].

One of the reasons for the limited knowledge on the active component structure – dispersion of supported Pt-oxygen mobility on and in the support – catalyst activity interrelationship is that short-contact-time and high-temperature reaction mechanisms are difficult to study. The method of studying the dynamics of product formation upon pulse feeding of the reagents at low pressure (Temporal Analysis of Products, TAP) seems to provide one of the most promising approaches for elucidation of mechanism [4,6]. This method allows assessing the effect of the oxidation level of a catalyst on its activity in the direct methane oxidation, which is a challenging problem in the case of fast reactions at atmospheric pressure. The TAP technique makes it possible to fix a certain oxidation level of a catalyst and then to test the reactivity of the latter by its exposure to small methane pulses which scarcely affect the surface. Since the quantities of reactants in a pulse are very small, the TAP technique allows evaluating the effect of the oxidation level of the surface without complicating thermal effects. Certainly, to verify the significance of mechanistic features of CPOM derived from TAP experiments for real-pressure processes, that data should be compared to steady-state characteristics of the catalyst activity and kinetic transients at ambient pressure [4]. To minimize the heat and mass transfer effects, supporting thin layers of active components either on the ceramic tube (annular reactor of Forzatti et al. [5]) or on walls of triangular channels cut from the corundum honeycomb substrates [12,13] was shown to be quite efficient approach for studies of POM reaction kinetic and mechanistic features in real feeds. Pulse studies at real concentrations of reagents, though strongly changing the surface oxygen coverage, could also be useful for estimating the rate of oxygen redistribution between the surface and subsurface layers [14,15], especially when combined with estimation of the heats of oxygen adsorption/methane oxidation or decomposition in a flow calorimeter [16,17].

This paper summarizes results of research aimed at elucidating effect of the surface/lattice oxygen mobility and reactivity for Pt-supported $Ln_{0.3}Ce_{0.35}Zr_{0.35}O_{2-y}$ (Ln = La, Pr, Gd) catalysts on their performance in POM at short contact times applying a complex of sophisticated kinetic methods. These catalysts containing 30 at.% of doping cation in ceria–zirconia solid solution were selected here due to close values of Pt dispersion combined with broadly varying surface oxygen mobility, which correlates with catalytic activity in POM in diluted feeds changing in the order La > Pr > Gd [11–13,18–24]. In this work the main attention is paid to elucidation and critical analysis of kinetic (especially, transient) features which might support or reject bifunctional scheme of POM mechanism with a due regard for the Pt-support interaction, oxygen transfer between Pt and surface sites/bulk of complex oxide supports and effect of realistic reaction feeds on the state of catalyst and its activity/syngas selectivity.

2. Experimental

2.1. Catalysts preparation

2.1.1. Powder catalysts

Samples were prepared according to the method yielding dispersed $Ln_x(Ce_{0.5}Zr_{0.5})_{1-x}O_2$ materials with Ln = La, Pr, or Gd content in the range of 5–30 at.% via a polymerized complex precursor route and successive calcinations at 500–900 °C for 4 h [4–6]. Pt (1.4 wt.%) was deposited from H_2PtCl_6 solutions by incipient wetness impregnation followed by drying and calcination at 700 °C for 2 h. Detailed characteristics of their structural and surface properties are given elsewhere [11,18–24].

2.1.2. Catalytic channels

A piece of a hollow thin-walled triangular prismatic corundum substrate (wall thickness 0.2 mm, inner triangle side 2.33 mm, length 10 mm) used in this work was cut from an α-Al_2O_3 honeycomb monolith annealed at 1300 °C (specific surface area 3 m^2/g). A layer of a $Ln_{0.3}Ce_{0.35}Zr_{0.35}O_{2-y}$ complex oxide was supported on this substrate by washcoating with the suspension made by ultrasonically dispersing the oxide powder in isopropanol with the addition of polyvinyl butyral. Several consecutive impregnations (typically 4) were required to attain the active component content of 7–10 wt.% (the porous layer thickness ca. 10 μm). After each impregnation, the samples were dried and calcined at 900 °C in air. Pt (1.4 wt.%) was supported by the incipient wetness impregnation with an H_2PtC_6 solution followed by drying and calcination at 900 °C in air.

2.2. Catalyst testing

CPOM tests were carried out in a plug-flow quartz reactor with the inner diameter of 6 mm. The space between the reactor walls and the catalyst channel was sealed up with α-Al_2O_3 fibers to provide the gas flow only through the channel. The catalyst was pretreated for 1 h in the flow of either O_2 at 700 °C (oxidizing pretreatment) or 30% H_2 in He at 900 °C (reducing pretreatment). The experiments were carried out at atmospheric pressure. The reaction mixture (7–20 vol.% CH_4, CH_4:O_2 = 2, N_2 balance) was fed in a flow rate range of 5.6–18.0 L/h corresponding to contact times of 4.7–15.0 ms as estimated from the flow rate and the volume of channel walls. The inlet and outlet temperatures of the catalyst channel were monitored during testing. Blank experiments with both the empty reactor and the reactor loaded with bare corundum substrate carrying no active component verified that homogeneous reactions did not occur under the studied conditions. The reagents and reaction products were analyzed with a quantitative analyzing gas chromatograph (Tsvet-500) as well as with calibrated on-line IR absorbance, electrochemical and polarographic gas sensors for

different components. In all the experiments, the carbon balance was close to 100 ± 5%.

Relaxation experiments at atmospheric pressure were performed in the same device in small quartz reactors. After preconditioning oxygen was flushed out with helium (control by the zero point of the oxygen sensor) and then helium was displaced with a required reaction mixture. The composition of the mixture was continuously analyzed by in-line gas sensors [4]. Control experiments with a single-channel fragment of the corundum carrier showed that, at gas flow rates of about 30 L/h, the purge time of the system during the concentration step up is no longer than 2–4 s.

2.3. Oxygen isotope heteroexchange

For powdered samples, experiments were carried out in the flow reactor using a SSITKA mode following earlier described procedures [10]. After achieving dynamic oxygen adsorption–desorption equilibrium at 500–700 °C, a flow of 1% $^{16}O_2$ in N_2 was switched for that of 1% $^{18}O_2$ in N_2, and concentrations of $^{16}O_2$, $^{16}O^{18}O$ and $^{18}O_2$ were monitored by the mass-spectrometer UGA 200 (Stanford Research Systems, USA).

For corundum channels with supported thin layer of Pr-doped active components, oxygen isotope exchange experiments were carried out in a closed reactor using a static installation (V = 680 cm^3) with on-line control of the gas phase isotope composition by QMS-200 (Stanford Research Systems, USA) mass-spectrometer both in the isothermal and the temperature-programmed mode (TPIE) (temperature ramp 5 K/min) in the temperature range 100–750 °C at $p(O_2)$ 1.5–4.5 Torr. The initial ^{18}O content in the gas phase was equal to 96%. Before experiments, samples were pretreated for 2 h under air at 650 °C for achieving a saturation of the solid phase with ^{16}O.

Parameters characterizing the rate of exchange, its mechanism and surface/bulk oxygen mobility were estimated from the data obtained in static or flow kinetic installations by using isotope-kinetic equations and analysis procedures described earlier in details [10,11,25,26].

2.4. Pulse studies

2.4.1. TAP experiments

The capability of the fully oxidized catalyst to react with methane was evaluated using the TAP system (TAP-1 reactor upgraded with a Stanford Research Systems, SRS RGA300 quadrupole mass spectrometer). The reactor was loaded with 20 mg of the powdered sample, evacuated and fed with a constant flow of 10% O_2 in Ne for reaching almost atmospheric pressure with closed high pressure assembly. Full oxidation of the catalyst and removal of hydrocarbon residuals was achieved by heating at 800 °C for 30 min in the flowing O_2/Ne mixture and successive cooling to 250 °C where the reactor was evacuated. Pulse experiments were conducted by stepwise increasing of the sample temperature and admission of a 25% CH_4 in Ar mixture with a pulse size of 2×10^{15} molecules per pulse. Pulse responses were recorded at characteristic masses of amu 2 (H_2), 15 (CH_4), 18 (H_2O), 28 (CO), 40 (Ar) and 44 (CO_2). Preliminary experiments revealed that the oxidized state of the catalyst could be preserved until a temperature of 525 °C before the thermal desorption of oxygen leads to a significant change of the catalyst. For quantitative analysis, the mass spectrometer was calibrated by reference experiments using the same experimental procedure over an inert quartz bed.

The TAP experiments were simulated with a one dimensional pseudo homogeneous model accounting for 3 zones (inert/active/inert) and temperature gradients in the inert sections. Calculations were performed by simultaneously solving the partial differential equations, denoting for the time (t) and space (z) dependency of concentration (c) and coverage (θ), with a FORTRAN program based on the method of lines. Assuming a non-reversible molecular Langmuir adsorption, the processes in the active zone are described by the partial differential equations for the gas phase oxygen (Eq. (1)) and adsorbed (Eq. (2)) species, respectively:

$$\frac{\partial c}{\partial t} = D_{\text{eff}} \cdot \frac{\partial^2 c}{\partial z^2} - \rho_S \cdot k_0 \cdot \exp\left(-\frac{E_a}{R \cdot T}\right) \cdot c \cdot (1-\theta) \quad (1)$$

$$\frac{\partial \theta}{\partial t} = k_0 \cdot \exp\left(-\frac{E_a}{R \cdot T}\right) \cdot c \cdot (1-\theta) \quad (2)$$

The kinetic parameters, site density ρ_s, frequency factor k_0 and activation energy E_a, were determined by their variation until the best possible fit between model prediction and experimental result had been achieved.

2.4.2. Ambient pressure pulse experiments

Pulse experiments were carried out using a Setaram Sensys DSC TG calorimeter and a pulse kinetic installation. The reagents and products concentrations were determined by a gas chromatograph "Chromos GH-1000". Sample 1.4% Pt/$Pr_{0.3}Ce_{0.35}Zr_{0.35}O_2$ (93 mg) was pretreated in the flow of 5% O_2 in He at 700 °C for 0.5 h and then in He for 0.5 h at the same temperature with subsequent cooling down in the He flow (flow rate 40 mL/min) to the temperature of experiments. Sample was reduced by pulses of 2% CO/He or 7% CH_4 in He (pulse volume 1–5 mL, time interval between pulses 15 min) removing several monolayers of oxygen.

2.5. Oxygen mobility/reactivity by temperature-programmed experiments

Experiments for temperature-programmed oxygen desorption in the flow of He (TPD O_2) and reduction of samples by CH_4 (1% CH_4 in He feed) were carried out in a flow installations equipped with quartz reactors, GC and PEM-2M gas analyzers under the temperature ramp of 5 °/min up to 880 °C with the isothermal plateau at 880 °C for 70 min [21,22].

3. Results and discussion

3.1. Steady-state catalytic activity in POM

Fig. 1 presents main characteristics of catalytic activity of corundum channels with supported active components. In all experiments, oxygen was completely consumed within the channel. For studied catalysts, CH_4 conversions at different contact times were satisfactorily fitted by the apparent first-order rate equation for the plug-flow reactor [13]. This implies that in studied experimental conditions variation of the gas-phase oxygen concentration profile with the superficial velocity has a weak impact on the rate constant of CH_4 transformation. Hence, in the first approximation, complete conversion of oxygen within channels does not obscure the difference between the intrinsic characteristics of catalytic activity of various active components supported on walls of corundum channels. This conclusion is also supported by the values of CH_4 conversion at short contact times being much lower than the equilibrium values (>90% at T > 700 °C) [12] as well as by a low (<30 °C) temperature gradient along the channel even for feed containing 20% CH_4. Reasonably high (~50 kJ/mol) activation energy of CH_4 consumption for Pr-containing catalysts possessing the highest activity at enhanced temperatures agrees with conclusion about negligible effect of heat and mass transfer on the catalyst performance in studied experimental conditions [12,13].

As follows from Fig. 1, at the lowest temperature range studied here the most active and selective is sample doped by La. This

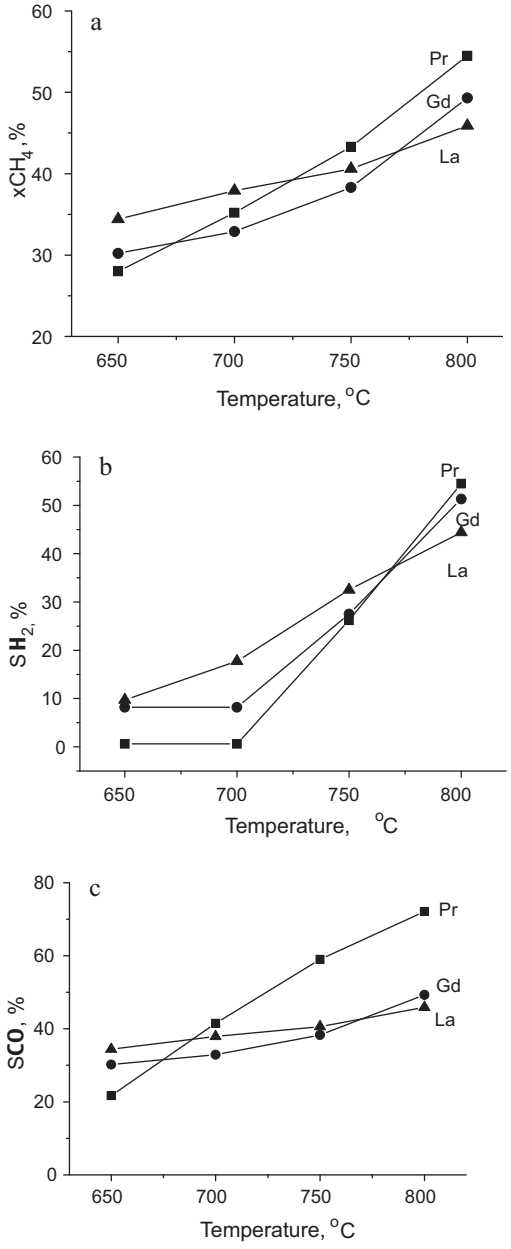

Fig. 1. Temperature dependence of CH_4 conversion (a), SH_2 (b) and SCO (c) for channels with Pt-supported supported ceria–zirconia oxides doped by Pr, Gd or La. Contact time 4.72 ms, feed 7% CH_4 + 3.5% O_2 in He.

agrees with results of experiments with diluted feeds carried out for powdered samples of Pt-supported doped ceria–zirconia solid solutions, where POM activity was shown to correlate with Pt dispersion and the surface oxygen mobility [24]. For La-doped sample, analysis of results of SSITKA experiments allowed to explain a high surface oxygen mobility by defects generated due to incorporation of Pt cations into the surface layer [10].

At highest temperatures, the most active and selective sample contains Pr as doping cation (Fig. 1). Analysis of oxygen isotope heteroexchange data for Pr-doped sample in a closed reactor revealed that indeed for this sample the oxygen bulk diffusion coefficient greatly exceeds that for La-doped sample [11]. Hence, at high temperatures, catalytic activity of Pt-supported doped ceria–zirconia catalysts appears to correlate with the lattice oxygen mobility. To verify this conclusion, the oxygen mobility in Pr-doped catalysts was studied in more details.

3.2. Oxygen isotope exchange

3.2.1. SSITKA

Fig. 2 presents data on the isotope fractions $\alpha_g(t)$ and $f_{34}(t)$ vs. time on stream as measured in SSITKA experiments over both $Pr_{0.3}Ce_{0.35}Zr_{0.35}O_2$ (Fig. 2a) and $Pt/Pr_{0.3}Ce_{0.35}Zr_{0.35}O_2$ (Fig. 2b) samples at 600 °C. Similar results were obtained at 500 and 700 °C.

The quantity of exchangeable oxygen in both samples as estimated from the difference in concentrations of labeled oxygen atoms at the reactor inlet and outlet ($N_O = (2C_{O_2}U/\alpha_g^{input}) \int_0^{t_{end}} (\alpha_g^{input} - \alpha_g)dt$) remains practically unchanged as the temperature rises and lies around 7×10^{21} at/g. This value is close to the stoichiometric content of oxygen in sample. Hence, in the course of isotope exchange, practically all ^{16}O in the sample was replaced by ^{18}O. As follows from this figure, Pt supporting increases the rate of oxygen exchange.

Numerical analysis of the dynamics of isotope transients carried out in frames of model [10] revealed that:

- The distribution of oxygen isotopes observed in these experiments corresponds to the mechanism of exchange with participation of two surface oxygen atoms denoted as K_3 [11,25] (cf. fitting by K_2 and K_3 mechanisms shown in Fig. 2).
- At temperatures below 600 °C, for both samples the rate of the lattice oxygen exchange is limited by the rate of the surface exchange. Rather fast oxygen diffusion provides a uniform distribution of labeled oxygen atoms in the bulk of oxide particles. Starting from 700 °C, the isotope exchange of oxygen in the bulk of oxide is controlled by the diffusion, which is the most clearly manifested for Pt-supported sample.

By fitting experimental curves, parameters of exchange model [10] were estimated (Table 1). Modeling results demonstrated that, similar to the majority of oxides, the mechanism of exchange involves interaction of O_2 molecule with two surface oxygen atoms, thus including the stage of O_2 dissociation [11,24,25]. The increase of the rate of exchange for Pt-supported sample is apparently caused by a fast O_2 dissociation on Pt followed by spillover of oxygen atoms to the oxide surface. Assuming that activity of oxide centers in the oxygen exchange is not changed due to Pt supporting ($R_{\text{oxide Pt/CeZrPrO}} = R_{\text{oxide CeZrPrO}} = K_{3\ \text{CeZrPrO}}$), the rate of exchange on Pt sites can be estimated:

$$R_{Pt} = \frac{(K_3 - R_{oxide})SL}{N_{Pt}}$$

Here N_{Pt} is the number of surface Pt atoms estimated to be ~10% of the total number of Pt atoms in sample [10,20–24]. Estimated values of R_{Pt} (Table 1) exceed those for oxide centers by two orders of magnitude despite good description of transients by the model of exchange on the uniform surface. This means that due to fast spillover and surface diffusion, labeled oxygen atoms are uniformly distributed on the surface of $Pt/CeZrPrO_x$. Apparently, to provide this result, the rate of spillover R_{sp} should substantially exceed the rate of exchange on Pt R_{Pt}. According to our estimation $R_{SPILL} \geq 2.5R_{Pt}$ (Table 1)

3.2.1.1. The mechanism of bulk oxygen diffusion. By taking the average particle radius $r = 3V/S = 6 \times 10^{-8}$ m (V – volume, S – specific surface area) as characteristic diffusion length, the bulk diffusion coefficient D is estimated to be $\approx 10^{-16}$ m^2/s. This value exceeds by several orders of magnitude known values for diffusion coefficients for ceria–zirconia oxides [26]. Such a phenomenon can be explained by specific structural features of studied nanocrystalline sample, namely, developed domain boundaries providing fast oxygen transfer from the surface of particle to the surface of domains

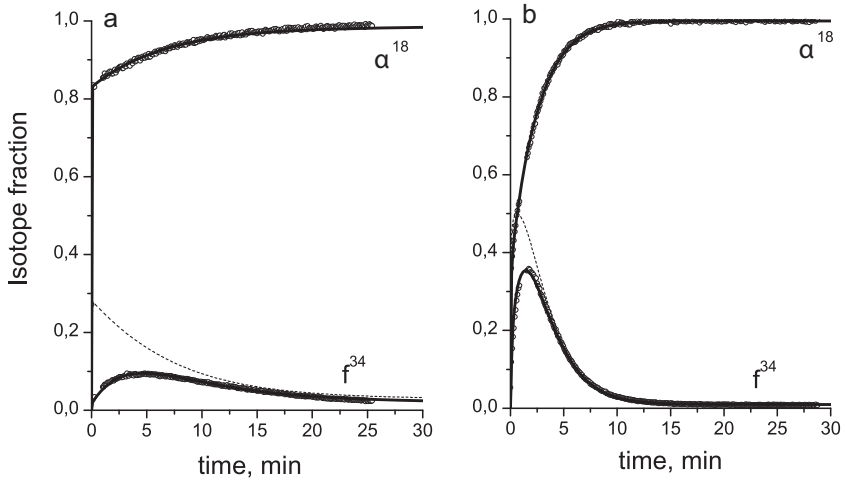

Fig. 2. Atomic fraction of ^{18}O in the gas phase (α) and fraction of $^{16}O^{18}O$ molecules (x_1) versus time of exchange for $Pr_{0.3}Ce_{0.35}Zr_{0.35}O_2$ (a) and 1.4% $Pt/Pr_{0.3}Ce_{0.35}Zr_{0.35}O_2$ samples (b). 600 °C, feed rate 300 mL/min, weight 0.05 g. Points – experiment, lines – fitting (dashed line by K_2 mechanism, solid line by K_3 mechanism).

[10,18–22]. Hence, dynamics of the isotope transfer into the bulk of oxide is controlled by the combination of two processes:

(a) by the surface diffusion of oxygen atoms along domains boundaries;
(b) by diffusion of oxygen atoms within the bulk of domains, their size determining diffusion length in this case.

According to structural data [20–24], the typical thickness of platelet-like domains in these samples is ca. 20 nm, so characteristic length $h \approx 10 \times 10^{-9}$ m. This allows to estimate the coefficients of oxygen diffusion in oxide domains D_{oxide} and along domain boundaries D_{mobile} from the effective coefficient of oxygen diffusion D_{eff} (Table 1):

$$D_{oxide} = D_{eff} \times h^2$$

$$D_{oxide} \geq D_{eff} \times r^2 \left(\frac{N_O}{N_{Omobil}} \right)$$

where N_{Omobil} is the number of oxygen atoms located within domain boundaries estimated to be ~5% of the total number of oxygen atoms in sample N_O. Estimated values of D_{oxide} and D_{mobile} for Pt/PrCeZrO sample are given in Table 1 along with parameters of oxygen exchange for Pt/LaCeZrO sample possessing the highest oxygen mobility for all series of La-doped samples [10]. While the constants of surface steps are close for both samples, the diffusion characteristics differ strongly. The rate of diffusion for La-doped sample was found to sharply decline with the particle depth due to specific structure and composition of the surface layers affected both by La and Ce surface segregation and Pt cations incorporation [20–24]. For Pr-doped sample, this phenomenon was not observed. Coefficients of oxygen diffusion within domains and along domain boundaries for this sample are higher than those for La-doped sample for 1 and 2 orders of magnitude, respectively.

Hence, results of SSITKA experiments confirm that Pr-doped sample indeed possesses much higher bulk oxygen mobility than La-doped sample, which agrees with its higher catalytic activity in the high-temperature range.

Since these results were obtained for powdered samples, oxygen isotope exchange in closed reactor has been carried out to verify that supporting active component on walls of corundum channel has not affected oxygen mobility.

3.2.2. *Oxygen isotope exchange for corundum channel with supported Pt/PrCeZrO$_x$ active component*

Fig. 3 shows typical results of oxygen isotope heteroexchange in closed reactor in the temperature-programmed (dynamic) mode. The depth of isotope penetration from the gas phase into the oxide in the course of TPIE can be characterized by the value N_X determined from the relation $2N\alpha^0 + N_X\alpha_S^0 = \alpha(2N + N_X)$. Here N is the number of O_2 molecules, N_X – number of oxygen atoms in solid, α^0 and α_S^0 – initial isotope fraction in the gas phase and solid, respectively.

Table 1
Parameters of oxygen exchange from SSITKA experiments.

T (°C)	Surface				Volume		
	K_3 (s^{-1})				D_{eff} (s^{-1})	D_{oxide} ($m^2\ s^{-1}$) × 10^{18}	D_{mobile} ($m^2\ s^{-1}$) × 10^{16}
	$Pr_{0.3}Ce_{0.35}Zr_{0.35}O_2$						
600	0.17				>0.02	>2	>14
700	0.25				>0.02	>2	>14
	1.4% $Pt/Pr_{0.3}Ce_{0.35}Zr_{0.35}O_2$						
	K_3 (s^{-1})	R_{oxide} (s^{-1})	R_{Pt} (s^{-1})	R_{sp} (s^{-1})			
400	0.02				>0.001	>0.1	>0.1
500	0.22				>0.01	>1	>8
600	0.5	0.17	11	≥30	>0.025	>2.5	>20
700	1	0.25	25	≥60	0.04	4	>33
	1.4% $Pt/La_{0.2}Ce_{0.4}Zr_{0.4}O_2$						
650	0.6	0.3	10	≥100	Bulk 0.004	0.4	0.45
					Sub. surf 0.04		0.7

Values of R_{Pt} and R_{sp} as calculated per Pt atom.

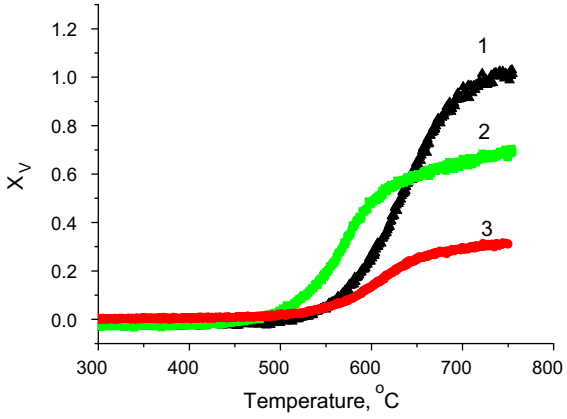

Fig. 3. Temperature dependence of the dynamic degree of exchange X_V for layers of $Pr_{0.3}Ce_{0.35}Zr_{0.35}O_x$ (1), $Pt/Pr_{0.3}Ce_{0.35}Zr_{0.35}O_x$ (2 and 3) supported on the walls of corundum channels. (1 and 2) Fresh samples, and (3) after testing in POM. PO_2 1.7–1.8 Torr.

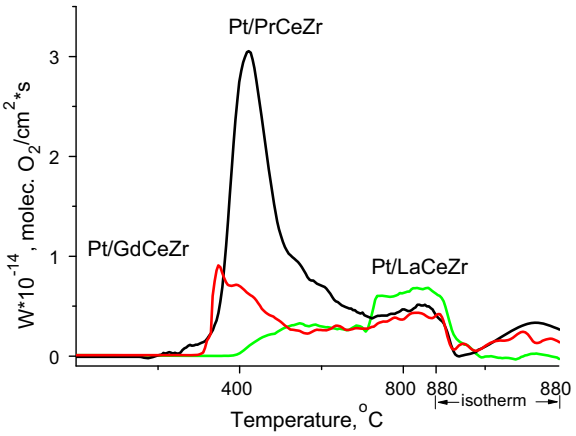

Fig. 4. O_2 TPD spectra for Pt/Ln–Ce–Zr–O samples calcined at 900 °C. Pretreatment in O_2 at 700 °C for 1 h.

The value $\mathbf{N_X}$ is related to the average depth of isotope incorporation into the solid phase ($\mathbf{l_\alpha}$) by relation $\mathbf{N_X = n_O \times S \times l_\alpha}$ (here $\mathbf{n_O}$ is the number of oxygen atoms in the unit volume of oxide). This quantity termed as "dynamic extent of isotope exchange" [18,24] is expressed here in relative units $X_V = (N_X/N_V)$, corresponding to the exchanged fraction of the bulk oxygen.

In agreement with SSITKA data for powdered samples, for Pr-doped ceria–zirconia oxide supported as a thin layer on corundum channel walls, all lattice oxygen is rather fast equilibrated with the gas-phase O_2. Pt supporting accelerates oxygen exchange at lower temperatures which is explained by a higher rate of exchange on Pt sites (vide supra). However, a slower increase of X_V at higher temperatures for Pt-promoted sample is not expected and could be explained by some variation of complex oxide properties caused by impregnation with acid H_2PtCl_6 solution, perhaps, caused by some leaching of aluminum cations from the corundum substrate. Even stronger and clearly negative effect is caused by catalyst testing in POM at high temperatures: both surface reaction and bulk oxygen diffusion are hampered. This is apparently caused by reduction of cationic forms of Pt incorporated into the surface layer of oxide followed by Pt aggregation. Subsequent reoxidation before oxygen exchange experiments apparently does not provide complete Pt redispersion.

Similar features as related to Pt supporting and reaction feed effect were observed in the isothermal exchange experiments (Table 2).

Hence, oxygen isotope heteroexchange experiments with catalytic channel demonstrated pronounced and irreversible reaction media effect on the oxygen mobility in Pt-supported catalysts. This effect might be much more pronounced for La-doped sample, which, along with a low bulk oxygen mobility, could explain its lowest activity at high temperatures.

3.3. Temperature-programmed O_2 desorption

Typical O_2 TPD spectra for samples pretreated in oxygen at 500 °C are shown in Fig. 4. The total amount of oxygen desorbed in TPD run varies from 14% monolayer (Pr) to 5–6% monolayer (Gd, La), thus corresponding only to a very small part of the total oxygen content in samples. Oxygen desorption from doped ceria–zirconia oxides without supported Pt starts in the same temperature range [22], hence, easily desorbed surface oxygen forms are bound not only with Pt cations but also with some surface defects on the surface of oxide particles as well. Moreover, oxygen desorption is accompanied by the oxygen diffusion along domain boundaries to the surface. With a due regard for the ^{18}O SSITKA data (vide supra), nearly all oxygen desorbed in TPD run can originate from domain boundaries. Indeed, a higher rate of oxygen desorption at ~400 °C from Pt/PrCeZr sample as compared with that for Pt/LaCeZr (Fig. 4) correlates with a higher coefficient of oxygen diffusion along domain boundaries for the former catalyst (Table 1).

3.4. Temperature-programmed reduction by CH_4

In these experiments, all reducible Me^{4+} cations (Ce^{4+}, Pr^{4+}) are reduced to Me^{3+} state after keeping under contact with CH_4 stream at 880 °C [22], which corresponds to removal ~10 monolayers of oxygen. Hence, reduction process is clearly associated with rapid oxygen diffusion from the bulk of oxide support particles to their surface where it is consumed by interaction with CH_x species generated by dissociation of CH_4 molecules on Pt sites. Such a dissociation continues at high temperatures even after nearly complete reduction of samples when CO_x evolution is practically not observed (Fig. 5).

The parallel evolution of CO, CO_2 and H_2 at ~400 °C (Fig. 5) for all oxidized samples demonstrates ability of these systems selectively transform CH_4 into syngas. The intensity of these low-temperature peaks clearly correlates with the surface/near-surface

Table 2
Oxygen isothermal exchange in a closed reactor for channels.

Sample	T (°C)	lg R, O_2 c^{-2} M^{-2}	E_a of heteroexchange (kJ/mol)	X_V^∞
$PrCeZrO_x$	650	17.0	110	0.54
	550	16.3		0.52
	500	15.8		0.56
$Pt/PrCeZrO_x$	650	17.2	90	0.42
	550	16.6		0.39
$Pt/PrCeZrO_x$ discharged from POM reactor	650	17.0	130	0.20
	600	16.6		0.22
	550	16.1		0.21

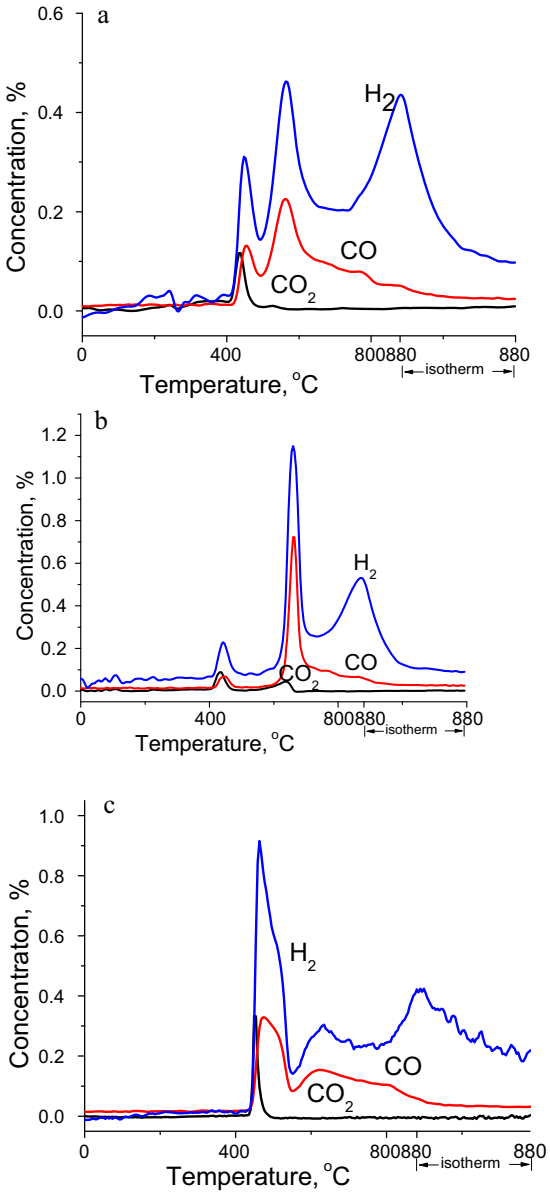

Fig. 5. CH_4 TPR spectra for Pt-supported ceria–zirconia oxides doped by Pr (a), Gd (b) or La (c).

oxygen mobility characterized by X_S (La > Pr > Gd) [11,18,24] and activity in both diluted feed [11] and concentrated feed (Fig. 1) at ~700 °C.

For Pr-doped sample the second peak of syngas evolution apparently controlled by the lattice oxygen diffusion and reactivity of strongly bound surface oxygen forms is situated at the lowest temperature (~550 °C) among studied samples. This apparently correlates with the highest catalytic activity of Pt/PrCeZrO in the high-temperature region in concentrated feeds (Fig. 1).

3.5. TAP

Quantitative exploitation of the recorded pulse responses indicated that for Pt/PrCeZrO sample a methane uptake occurs at temperatures higher than 360 °C, which agrees well with results of CH_4 TPR (Fig. 5). It is important to note that there is no pulse broadening at lower temperatures, which would be expected when methane could adsorb. Hence, it can be concluded that methane reacts as soon as it adsorbs. Furthermore, the oxidized state of the catalyst is crucial to activate methane as highlighted by the fact that catalyst pretreated at 800 °C in vacuum or reduced by hydrogen does not significantly activate methane in the temperature range between 360 and 525 °C. Most likely the methane activation over the fully oxidized catalyst proceeds according to an oxygen-assisted mechanism.

The result of the parameter estimation according to the simple model of irreversible molecular Langmuir adsorption for Pt/PrCeZrO sample can be summarized as follows:

site density $\rho_s = 3.4$ mol/m^3_{cat};
frequency factor $k = 68.6\ s^{-1}$ at 923 K;
activation energy $E_a = 65.9$ kJ mol^{-1}.

The activation energy of POM for this sample in real feeds (ca. 50 kJ/mol [13]) is rather close for that of CH_4 irreversible adsorption. This suggests that the stage of activated CH_4 adsorption is rate-limiting.

It should be noted that the match of the simulated and the experimental responses decreases at temperatures higher than 686 K. In parallel, first responses for CO_2 were recorded above this temperature. Obviously, a model accounting for the conversion of adsorbed methane could lead to a more suitable description of the methane responses. On the other hand, CO_2 responses were broad and had a low peak intensity thus requiring additional experimental efforts in order to reach a signal quality sufficient for further parameter estimation.

The performance of the fully oxidized Pt/PrCeZrO_x catalyst at 670 °C was established by pulse experiments supplying a 25% CH_4 in Ar mixture. However, at this temperature oxygen desorbs from the catalyst (see Fig. 4) and is only partially resupplied from the bulk of PrCeZrO_x particles. Hence, the availability of the most reactive oxygen species on the surface decreases with time. This decline in the oxygen surface concentration is clearly reflected by the increasing intensity of CH_4 pulse responses with time, i.e. a lowering of the CH_4 conversions reflected in the responses from the back to the foreground. Obviously, the CH_4 activation is oxygen assisted given the higher conversions are achieved at a higher degree of oxidation. Focusing on the responses for the products CO_2 and CO, with the latter being obtained from the responses at amu 28 and subtraction of the contribution of CO_2 on this amu, it comes clear that CO is a primary product with very sharp responses, while CO_2 as secondary product shows much broader pulse responses. Furthermore, CO_2 has a maximum yield at a high degree of oxidation, while the maximum yield of CO is only achieved after some oxygen was removed from the catalyst surface by desorption. These findings are indeed perfectly in line with the above mentioned assignment of CO being the primary product of the CH_4 partial oxidation and CO_2 being then formed from CO by over-oxidation.

3.6. Pulse reduction experiments at realistic CH_4 concentrations

In general, variation of CH_4 conversion and CO/CO_2 selectivity with the pulse number (degree of sample reduction) observed in these experiments (Fig. 7) reasonably agrees with that for TAP data (Fig. 6). The CO formation even for the first pulse of CH_4 supplied to the oxidized sample surface supports hypothesis about a primary route of syngas formation via a CH_4 pyrolysis-partial oxidation route. Rather high degrees of CH_4 conversion after removal from the sample ~ monolayer of oxygen clearly demonstrate a high rate of oxygen diffusion from the bulk of oxide particle to the surface. The average heat of oxygen adsorption on partially reduced surface (~600 kJ/mol O_2, Fig. 8) is close to values corresponding to bonding strength of bridging (M_2O) oxygen forms located at Ce cations [27]. Its weak variation with the reduction degree can be explained by dynamic equilibrium between on-top (terminal) M–O oxygen

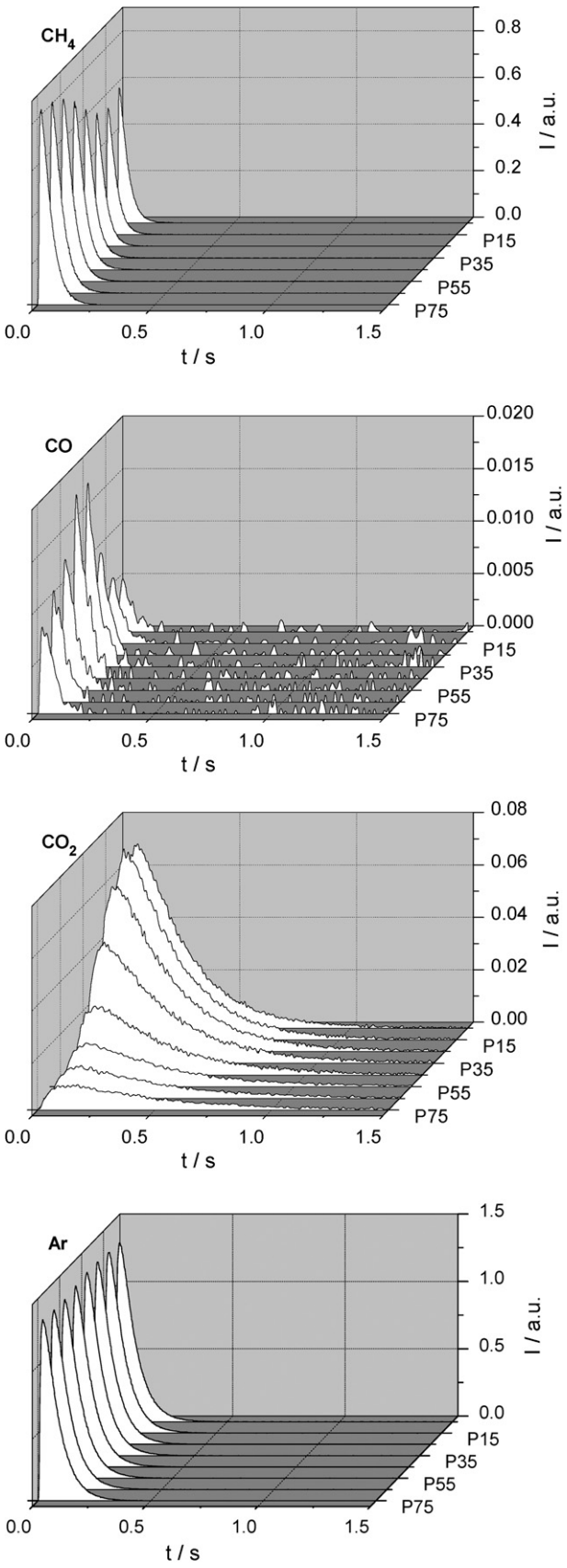

Fig. 6. Three-dimensional representations (intensity–time–pulse number) of the pulse responses for CH_4, CO_2, CO and Ar (reference gas) at 670 °C after oxidizing pretreatment.

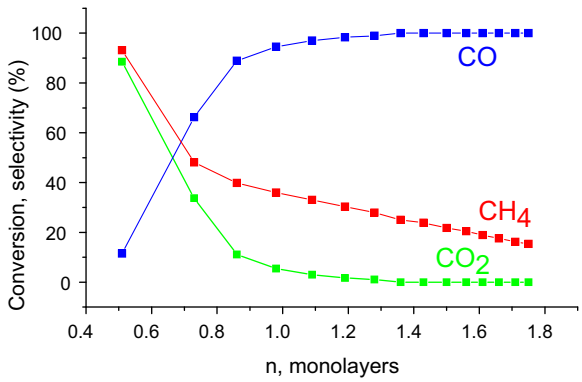

Fig. 7. Dependence of CH_4 conversion, CO and CO_2 selectivity on the degree of Pt/PrCeZrO sample reduction (n) by pulses of 7% CH_4 in He at 600 °C.

forms (average heats of adsorption for ceria–zirconia solid solutions ~300–500 kJ/mol O_2 [27]) supplied to the surface by diffusion from the bulk of particles and bridging M_2O oxygen forms as considered within the frames of so called partially flexible model of the surface [28]. The main point of this model is that reduction of oxide sample via removal of bridging oxygen forms could increase the density of surface sites for stabilization of less strongly bound terminal oxygen forms via rearrangement of the real/defect structure. For ceria–zirconia solid solutions this possibility appears due to formation of fragments with pyrochlore-type structure in the course of reduction where coordination of Zr cations changes from 8-fold to octahedral one. A partial reoxidation of the surface layer by oxygen migrating from the bulk of oxide particle could thus generate oxygen interstitials in the subsurface layer with associated surface site for oxygen stabilization in the moderately bound on-top form [27].

The enthalpy of CH_4 interaction with the catalyst (Fig. 9, endothermic process) increases with the reduction degree corresponding to the enthalpy of its transformation into deep and partial oxidation products with a due regard for syngas selectivity and variation of the average oxygen bonding strength. Some decline of the heat of reduction at reduction degree exceeding 1.5 monolayer can be explained by increasing contribution of CH_4 pyrolysis in agreement with results of CH_4 TPR data (Fig. 5). Nearly linear (i.e., rather weak) dependence of CH_4 conversion on the reduction degree agrees with this weak variation of the heat of CH_4 transformation. Hence, the rate of CH_4 transformation in studied range of sample reduction degree is mainly determined by the surface coverage with reactive terminal oxygen forms replenished between pulses via diffusion from the bulk of oxide particles to the surface.

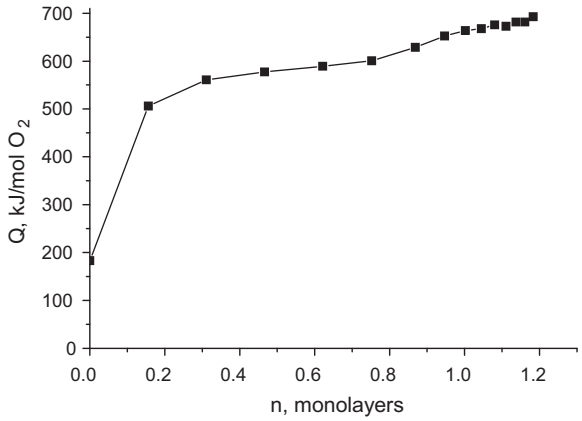

Fig. 8. Enthalpy of oxygen adsorption (Q) versus reduction degree (n) estimated from the heats of 1.4% Pt/$Pr_{0.3}Ce_{0.35}Zr_{0.35}O_2$ sample reduction by CO pulses at 600 °C.

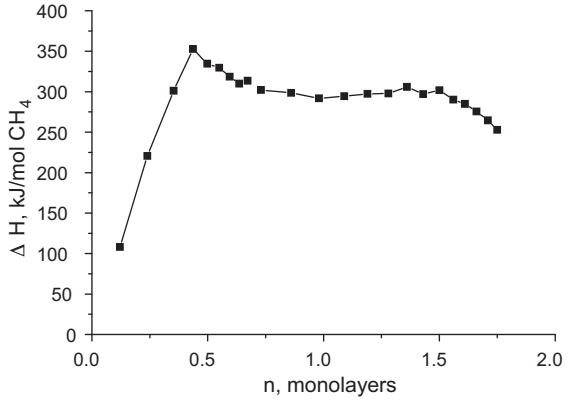

Fig. 9. Enthalpy of CH_4 interaction with 1.4% $Pt/Pr_{0.3}Ce_{0.35}Zr_{0.35}O_2$ sample as a function of reduction degree (n) at 600 °C.

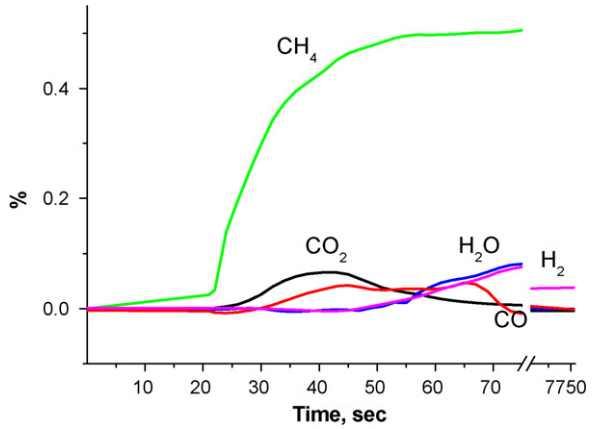

Fig. 11. Transients in the course of $Pt/Pr_{0.3}CeZrO_x$ channel reduction by 0.5% CH_4 in He at 700 °C after pretreatment in He. Contact time 5 ms.

Since the rate of the surface diffusion (reverse oxygen spillover from the support to Pt) is high, this provides some coverage of Pt by adsorbed oxygen thus helping in the activation of CH_4 molecules.

3.7. Kinetic transients for separate structured catalytic elements (channels)

3.7.1. Interaction with CH_4

Kinetic analysis of results of catalysts reduction by pulses of CH_4 at realistic concentrations in the flow reactors is known to be complicated by inevitable time lag between pulses required for the products analysis, indefinite regime of gas flow through the layer of a powdered catalyst (radial and back flow mixing, etc.), impact of the mass and heat transfer, etc. [14–17]. These problems were mainly avoided while using a continuous flow through the reactor equipped with a separate structural catalytic element – corundum channel with the active component supported on its walls [12,17,29,30]. Hence, a series of experiments for elucidating the effect of mild reducing pretreatment on kinetic features of CH_4 interaction under real-pressure conditions with the Pt/PrCeZrO catalyst supported on the corundum channel walls have been carried out. The main aim of these experiments was to verify conclusion of TAP studies about importance of oxidation state of Pt and oxygen transfer from support to Pt sites for the primary transformation of CH_4 into syngas.

Figs. 10 and 11 present results of transient studies when the stream of He was switched at 700 °C for that containing 0.5% CH_4 in He. For the catalyst pretreated in O_2, results apparently support conclusion of high-vacuum TAP studies. CO appears at the reactor outlet simultaneously with CH_4 corresponding to behavior of the primary product, while CO_2 curve is delayed as should be for the secondary product. Hydrogen is delayed even more suggesting its fast oxidation by reactive oxygen species. Primary route of CH_4 activation on oxidized Pt sites producing CO and hydroxyls (or water) could not be excluded as well.

Catalyst pretreatment in He removing rather small amount of oxygen located at the surface sites and within domain boundaries (vide supra) strongly deactivates it which also agrees with results of TAP studies. CH_4 is more strongly adsorbed on the surface of mildly reduced catalyst, and its subsequent transformation is accompanied by appearance of first CO_2 then CO and hydrogen when the surface is more reduced. Hence, presence of the mobile surface/near surface oxygen and oxidized Pt species not only helps to activate methane but also affects the mode of its primary transformation into products of partial or deep oxidation.

3.7.2. Interaction with $CH_4 + O_2$ stream

Addition of 0.5% O_2 to the feed 1% CH_4 in He strongly affects transients (Figs. 12 and 13). Apparently gas-phase or weakly bound oxygen species provide fast combustion of the products of CH_4 activation on oxidized Pt sites, so CO_2 and H_2O appear first. Subsequent appearance of hydrogen and later CO accompanied by the increase of CH_4 consumption is associated with the sample reduction along with carbonization and hydroxylation of the surface layer. Hence, at low CH_4 concentrations in the feed, gas-phase oxygen increases the rate of oxidation of activated CH_x species, apparently via increase

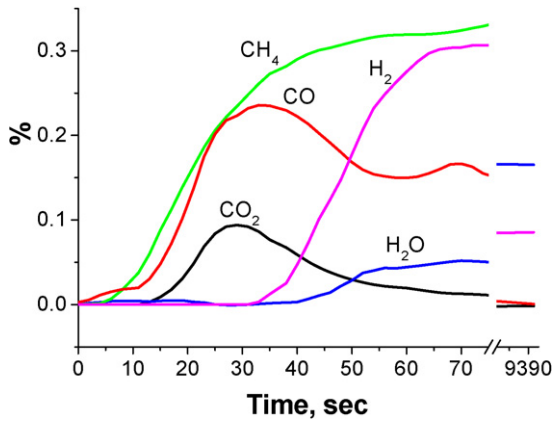

Fig. 10. Transients in the course of $Pt/Pr_{0.3}CeZrO_x$ channel reduction by 0.5% CH_4 in He at 700 °C after pretreatment in O_2. Contact time 5 ms.

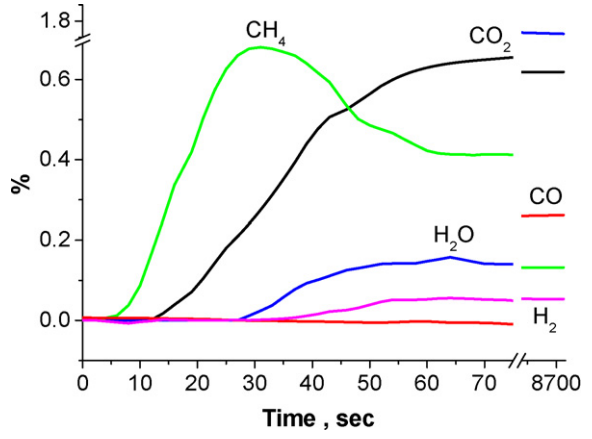

Fig. 12. Transients in the course of $Pt/Pr_{0.3}CeZrO_x$ channel contact with the feed 1% CH_4 + 0.5% O_2 at 700 °C after pretreatment in O_2. Contact time 5 ms.

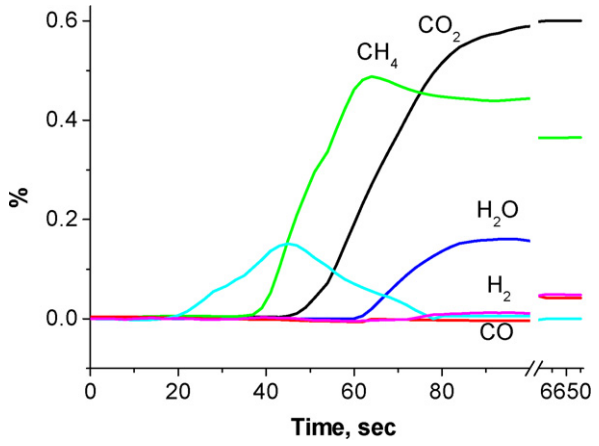

Fig. 13. Transients in the course of $Pt/Pr_{0.3}CeZrO_x$ channel contact with the feed 1% CH_4 + 0.5% O_2 at 700 °C after pretreatment in He. Contact time 5 ms.

of the rate of reverse oxygen spill-over from the oxide sites to Pt. Similar results were obtained in TAP experiments when decreasing the time lag between the oxygen and methane pulses resulted in a lower syngas selectivity [4].

Pretreatment in He strongly deactivates sample with respect to interaction with diluted $CH_4 + O_2$ feed (Fig. 13), which agrees with results presented in Section 3.7.1. Hence, the main factor is apparently a low reactivity of more reduced and/or more aggregated supported Pt species. It is noteworthy that even prolonged contact of sample pretreated in He with diluted reaction feed does not allow to achieve syngas yield equal to that for sample pretreated in O_2. This suggests that Pt aggregation caused by the high-temperature pretreatment in He is accompanied by catalyst deactivation, either due to decrease of Pt-support interface or by rearrangement of the structure of oxide surface or that of domain boundaries hampering oxygen diffusion.

For the same active component, transients in realistic concentrated $CH_4 + O_2$ feed (Fig. 14) revealed substantial difference with those observed for diluted feed (Fig. 12). In concentrated feed simultaneous appearance of CH_4 and products of its partial and deep oxidation clearly suggests realization of the primary route of CH_4 transformation into syngas followed by subsequent oxidation of CO and H_2 in the inlet part of the channel where the gas phase oxygen is present. A slow decline of exit CO_2 concentration with time accompanied by the increase of syngas yield (Fig. 14) is apparently caused by the partial reduction of catalyst by reaction feed similar to the case of oxygen-pretreated catalyst in diluted feed (Fig. 12). Hence, the key difference with diluted feed is that for the oxidized surface syngas selectivity in concentrated feed is much higher. In general case, it can be explained by interplay of several factors including pure kinetic ones (different kinetic orders of CH_4 and oxygen adsorption), mass transfer limitations for O_2 consumption [3] and variation of the catalytic properties of supported Pt, surface sites of complex oxide and Pt-support interaction as dependent upon the feed composition due to fast accumulation of some intermediates (CH_xO species), hydroxyls and carbonates. At least suggestion about different kinetic orders of CH_4 and O_2 adsorption (1 and 0, respectively) agrees well with a weak adsorption of CH_4 by TAP data (vide supra) as well as the POM order in CH_4 ~1 in realistic feeds demonstrated in experiments with channel-supported catalysts [12,13].

At longer contact times (Fig. 15) for the same feed composition transient characteristics are rather similar with the exception of some delay in CO appearance. By analogy with results for diluted feed (Fig. 12), this feature can be explained by faster oxidation of CO as compared with hydrogen in the inlet part of the channel. Since

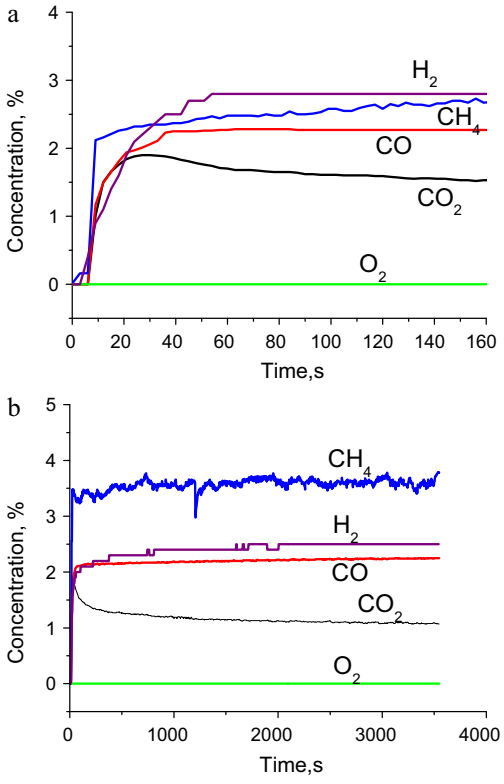

Fig. 14. Typical kinetic transients for channel with $Pt/PrCeZrO_x$ active component after oxidizing pretreatment. (a) Initial period and (b) slow transients. 750 °C, contact time 3.54 ms, feed 7% CH_4 + 3.5% O_2 in He.

at longer contact times oxygen is expected to be consumed within a narrower inlet part of the channel, subsequent CH_4 steam and dry reforming reactions as well as water gas shift reaction can also affect both dynamics of CO evolution as well as its steady-state concentration. However, sample pretreatment in hydrogen (Fig. 15c) revealed that reduced surface is much less reactive with respect to CH_4 than the oxidized one, so steam and dry reforming reaction occurring under the initial moments of reaction feed contact with oxidized catalyst surface are certainly to be much slower than the partial oxidation providing only a moderate increment to the methane conversion in the steady-state conditions at high temperatures [12,13]. This conclusion agrees with direct estimations of the rate constants of CH_4 steam and dry reforming on these catalysts which were shown to be several times lower than those of POM in feeds with realistic CH_4 content [29,30].

Dynamics of transients for reduced sample (Fig. 15c) clearly demonstrates that the gas phase or physically adsorbed oxygen species do not play any noticeably role in deep or partial oxidation of methane – all products appear after delay required for sample oxidation. Moreover, Pt aggregation caused by sample pretreatment with hydrogen (and, hence, weakened Pt-support interaction) only deteriorates syngas selectivity.

For Gd-doped catalyst kinetic transients in real feeds are rather similar to those for Pr-doped one (Fig. 16). During initial period (Fig. 16a) CO and CO_2 appear simultaneously with methane which agrees with primary route of methane transformation into syngas. The most pronounced difference with Pr-doped sample consists in a slow decline of syngas concentration with time-on-stream. At lower temperatures (650 °C), for Pt/GdCeZr catalyst decline of exit concentration of CO and H_2 with time-on-stream from the maximum to a steady-state level was much stronger (by three times) than for Pt/PrCeZr sample (<25 rel.%) [4]. For La-doped sample a similar slow decline of CO and H_2 concentrations with time-on-

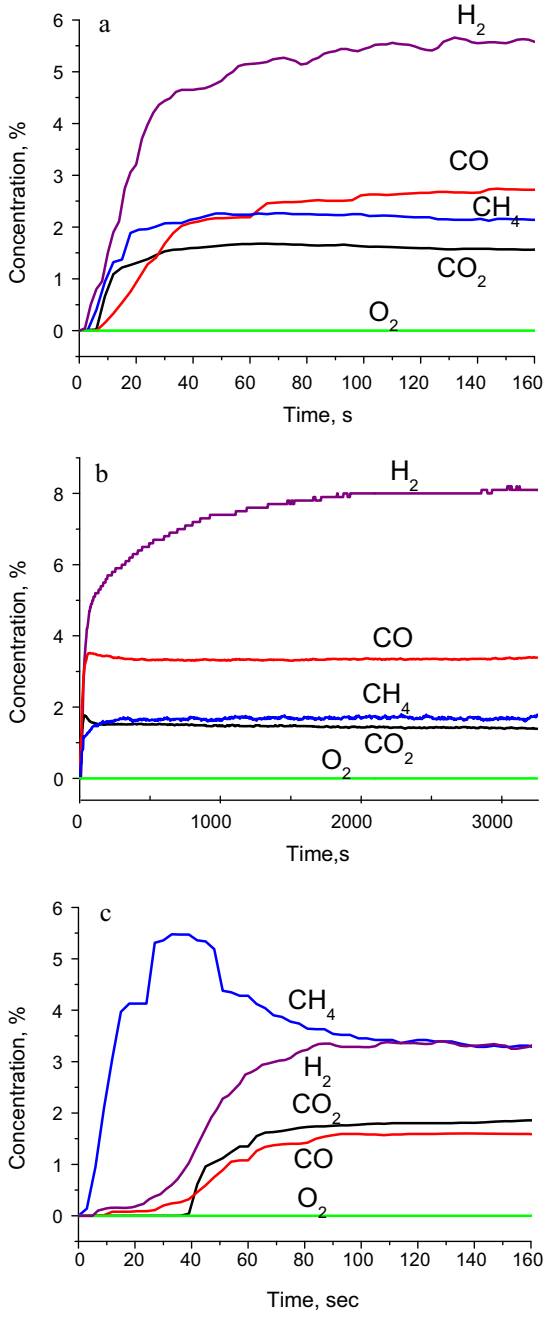

Fig. 15. Typical kinetic transients for channel with $Pt/PrCeZrO_x$ active component after oxidizing (a and b) or reducing (c) pretreatment. (a and c) Initial period and (b) slow transients. 750 °C, contact time 15 ms, feed 7% CH_4 + 3.5% O_2 in He.

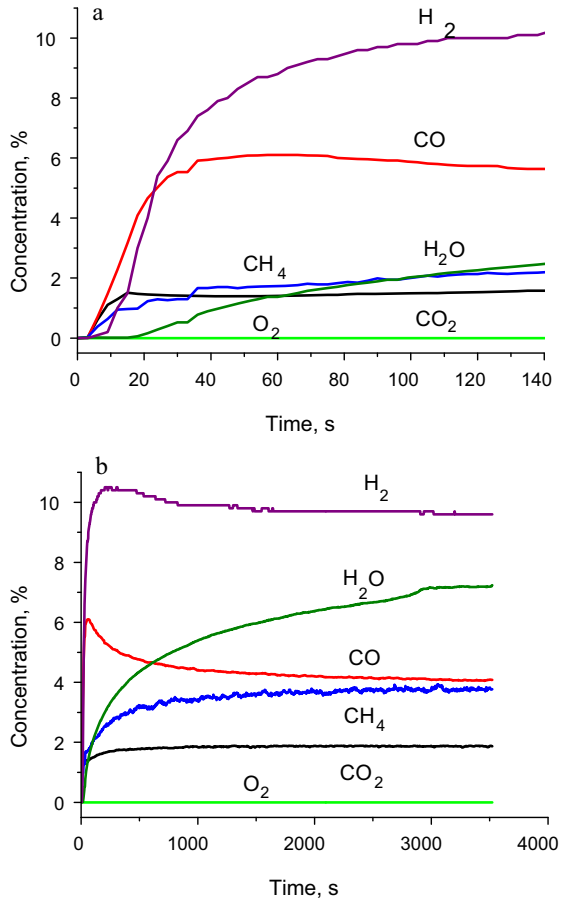

Fig. 16. Typical kinetic transients for channel with $Pt/GdCeZrO_x$ active component after oxidizing pretreatment. (a) Initial period and (b) slow transients. 750 °C, contact time 15 ms, feed 10% CH_4 + 5% O_2 in He.

stream was observed (Fig. 17), being also much stronger at 650 °C. Since the most clear difference between Pr- and Gd- or La-doped samples consists in the much higher bulk oxygen mobility for the former sample, this result supports conclusion about importance of lattice oxygen mobility to provide a high and stable performance of Pt-supported doped ceria–zirconia oxides in POM.

3.8. Basic steps of reaction mechanism

While detailed analysis of kinetic transients for POM in concentrated feeds on channels is still in progress (to be presented elsewhere), basic features of these transients are qualitatively similar to those studied earlier for powdered Pt/CeZrO and Pt/LaCeZrO catalysts in more diluted feed (4.6% CH_4 + 2.2% O_2 in He) [7,22,24].

Moreover, constants obtained by such an analysis combined with published data on the elementary steps of POM mechanism were successfully applied for description of steady-state and transient regimes of POM on monolithic catalysts with this type of active component [31]. Hence, it seems to be reasonable and useful to present here constants of some lump steps of the microkinetic POM scheme estimated for studied types of catalysts [7,32,33] (Table 3) as a basis for more detailed discussion of the effect of the oxygen mobility and metal-support interaction on the activity and stability in POM.

The most important point here is that the rate constant of step 5 (selective oxidation of CH_4 into syngas by PtO) is comparable with

Table 3
Basic microkinetic steps of the mechanism of CH_4 partial oxidation on $Pt/LnCeZrO_x$ catalysts [7,31].

No.	Step	K at 650 °C (s^{-1})
1	$O_2 + 2Pt \leftrightarrow 2PtO$	10^4
2	$H_2O + z \leftrightarrow H_2 + zO$	1.5
3	$zO + Pt \leftrightarrow PtO + Z$ spillover	>50
4	$O_{bulk} + z \leftrightarrow zO + V_O$ (bulk) diffusion	>10 along domain boundaries
5	$CH_4 + PtO \rightarrow CO + 2H_2 + Pt$	10^4
6	$CH_4 + 4PtO \rightarrow CO_2 + 2H_2O + 4Pt$	10^2
7	$CO + PtO \rightarrow CO_2 + Pt$	3.5×10^2
8	$H_2 + PtO \rightarrow H_2O + Pt$	$<1 \times 10^2$
9	$Pt + CO + H_2O \leftrightarrow CO_2 + H_2 + Pt$	$>10^4$ WGS reaction by associated mechanism

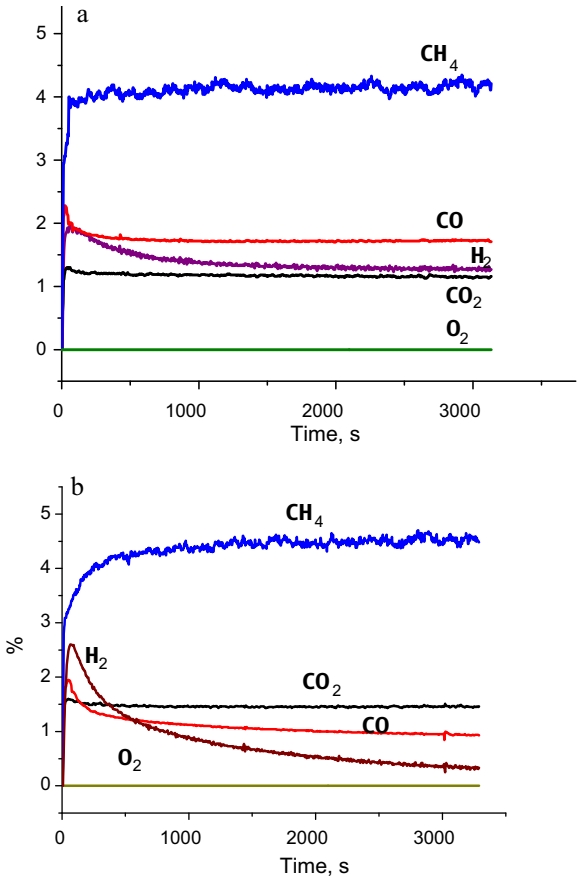

Fig. 17. Typical kinetic transients for channel with Pt/LaCeZrO$_x$ active component after oxidizing pretreatment. (a) 750 °C and (b) 650 °C. Contact time 4.72 ms, feed 7% CH_4 + 3.5% O_2 in He.

that for the oxygen adsorption (step 1) and exceeds much those for CH_4 combustion (step 6) and CO and H_2 oxidation (steps 7 and 8). This feature clearly explains syngas generation on these types of Pt-supported catalysts even in the presence of gas-phase oxygen. For Rh and Pt catalysts, either bulk or supported on irreducible oxides (alumina, MgO, etc.) [5,34] the situation is reversed, and indirect route of syngas formation is realized due to much faster combustion and CO/H_2 oxidation in the presence of gas-phase oxygen. Hence, strong Pt-support interaction, which results in domination of cationic forms of Pt for studied systems [18–22], provides radical variation of the chemical reactivity of supported Pt enhancing its reactivity in methane transformation along selective route of syngas generation while suppressing its combustion activity. This would be rather expected since combustion requires at least several available surface oxygen atoms adsorbed on a cluster comprised of several Pt atoms. Moreover, sticking coefficients and reactivity of CO and H_2 are well-known to be much lower for the oxygen covered Pt surface [35].

From the point of view of this scheme, a high rate of surface/bulk oxygen diffusion helps to stabilize Pt in the oxidized state thus preventing its aggregation leading to increase of combustion activity. In turn, a high Pt dispersion provides developed Pt-support interface required for the efficient reverse oxygen spill-over from support to Pt. Though rate constants of the surface diffusion and spill-over are smaller that those of oxygen adsorption and consumption (stages 5–8), nevertheless, when the latter rates are comparable, and, hence, their difference is small, stages of surface/bulk diffusion could noticeably affect the oxygen coverage of Pt sites, and, hence, activity and syngas selectivity. In the part of the channel where oxygen is absent, fast water gas shift reaction (Table 3) apparently occurs even at short contact affecting products distribution.

Another point is that for partially reduced support containing Ce and Pr cations, adsorption and dissociation of O_2 on the oxide vacancies as well as their reoxidation by water (stage 2) provide required replenishment of surface species to provide continuous oxygen flux to Pt-support interface. Certainly, the role of support is more complex including stabilization of some intermediates such as formates [36], or spectators such as carbonates affecting the surface oxygen mobility/reactivity, especially at lower temperatures, which requires further studies.

Certainly, conclusion of this work about important role played by highly dispersed Pt oxidic species stabilized due to Pt-support interaction requires further detailed studies aimed at their detection and characterization under real operation conditions applying *in situ* spectroscopic techniques with a due regard for the oxygen concentration gradient along the catalytic bed/channel length and its variation with the temperature and feed rate. Raman spectroscopy [22,37] and XANES/EXAFS [38–40] were shown to be among the methods the most sensitive to the oxidation state of Pt group metals and compatible with design of catalytic microreactors. Thus, X-ray absorption spectroscopy revealed that even for Rh (Rh + Pt)/Al_2O_3 catalysts with a rather moderate metal-support interaction, after ignition of CH_4 partial oxidation into syngas the Rh and Pt are mainly in the oxidized state in the narrow entrance zone of the catalytic bed and in the metallic state towards the end of the bed [38–40]. Some modification of the Pt-supported structured catalyst design (i.e., supporting catalytic layer on the wall of a quartz capillary for Raman studies, etc.) would be required as well for such future studies to provide required spatial resolution.

4. Conclusions

The combination of information on structural properties revealed by detailed characterization and kinetic information obtained at relevant conditions by various transient techniques allowed to rationalize the unique reactivity of Pt deposited on optimized supports with OSC. The selective oxidation of methane into syngas at short contact times on Pt-supported lanthanide doped ceria–zirconia catalysts was shown to proceed through direct route with oxygen-assisted methane activation on Pt. This is contrary to conventional catalysts having Pt deposited on support materials without significant oxygen mobility. Hence, catalysts with OSC supports and high oxygen surface mobility present relevant feature to allow conducting the CPOM reaction according to a bifunctional mechanism. The specific catalytic performance seems provided by strong Pt-support interaction stabilizing highly dispersed oxidic Pt species less active in CH_4 and syngas combustion than bulk Pt. It seems reasonable assuming that a limited coverage of electrophilic oxygen on the Pt surface and the dominant course of the reaction at the interface between Pt and the support interface manifests macroscopically in the primary formation of synthesis gas. Additionally, a high rate of surface/bulk oxygen diffusion and Pt-support oxygen spillover stabilizes these species while preventing coking.

Acknowledgements

This work was carried out in frames of Russian-French Associated European laboratory on catalysis. Support by OCMOL FP7 Project, RFBR–CNRS 09-03-93112 Project and Russian Federal Innovation Agency via the program “Scientific and Educational cadres” is gratefully acknowledged. The DFG collaborative research center SFB558 is kindly acknowledged for supporting the research stay of E. Gubanova. The Embassy of France in Moscow is

gratefully acknowledged for the joint PhD studentship grant of A. Bobin.

References

[1] J. Haber, Stud. Surf. Sci. Catal. 110 (1997) 1.
[2] D.A. Hickman, L.D. Schmidt, Science 259 (1993) 343.
[3] E.L. Gubanova, Y. Schuurman, V.A. Sadykov, C. Mirodatos, A.C. van Veen, Chem. Eng. J. 154 (2009) 174.
[4] E.L. Gubanova, A. van Veen, C. Mirodatos, V.A. Sadykov, N.N. Sazonova, Russ. J. Gen. Chem. 78 (2008) 2191.
[5] A. Donazzi, A. Beretta, G. Groppi, P. Forzatti, J. Catal. 255 (2008) 241.
[6] E.L. Gubanova, V.A. Sadykov, A.C. van Veen, C. Mirodatos, React. Kinet. Catal. Lett. 97 (2009) 349.
[7] C. Mirodatos, Y. Schuurman, A.C. van Veen, V.A. Sadykov, L.G. Pinaeva, E.M. Sadovskaya, Stud. Surf. Sci. Catal. 167 (2007) 287.
[8] E. Odier, Y. Schuurman, K. Barral, C. Mirodatos, Stud. Surf. Sci. Catal. 147 (2004) 79.
[9] M. Fathi, F. Monnet, Y. Schuurman, A. Holmen, C. Mirodatos, J. Catal. 190 (2000) 439.
[10] E.M. Sadovskaya, Y.A. Ivanova, L.G. Pinaeva, G. Grasso, T.G. Kuznetsova, A. van Veen, V.A. Sadykov, C. Mirodatos, J. Phys. Chem. A 111 (2007) 4498.
[11] V. Sadykov, V. Muzykantov, A. Bobin, N. Mezentseva, G. Alikina, N. Sazonova, E. Sadovskaya, L. Gubanova, A. Lukashevich, C. Mirodatos, Catal. Today 157 (2010) 55–60, doi:10.1016/j.cattod.2010.03.064.
[12] N.N. Sazonova, V.A. Sadykov, A.S. Bobin, S.A. Pokrovskaya, E.L. Gubanova, C. Mirodatos, React. Kinet. Catal. Lett. 98 (2009) 19.
[13] N.N. Sazonova, V.A. Sadykov, A.S. Bobin, S.A. Pokrovskaya, E.L. Gubanova, C. Mirodatos, React. Kinet. Catal. Lett. 98 (2009) 27.
[14] V.A. Sadykov, T.G. Kuznetsova, S.A. Veniaminov, D.I. Kochubey, B.N. Novgorodov, E.B. Burgina, E.M. Moroz, E.A. Paukshtis, V.P. Ivanov, S.N. Trukhan, S.A. Beloshapkin, Yu.V. Potapova, V.V. Lunin, E. Kemnitz, A. Aboukais, React. Kinet. Catal. Lett. 76 (2002) 83.
[15] C. Batiot-Dupeyrat, G. Valderrama, A. Meneses, F. Martinez, J. Barrault, J.M. Tatibouet, Appl. Catal. A: Gen. 248 (2003) 143.
[16] Yu. Bychkov, Yu. Tulenin, O. Krylov, V. Korchak, Kinet. I Katal. 43 (2002) 775.
[17] Yu. Bychkov, Yu. Tulenin, O. Krylov, V. Korchak, Kinet. I Katal. 44 (2003) 384.
[18] V.A. Sadykov, N.V. Mezentseva, G.M. Alikina, A.I. Lukashevich, Yu.V. Borchert, T.G. Kuznetsova, V.P. Ivanov, E.A. Paukshtis, V.S. Muzykantov, V.L. Kuznetsov, V.A. Rogov, J. Ross, E. Kemnitz, C. Mirodatos, Solid State Phenom. 128 (2007) 239.
[19] V. Sadykov, E. Kriventsov, E. Moroz, Yu. Borchert, T. Kuznetsova, V. Ivanov, A. Boronin, N. Mezentseva, E. Burgina, J. Ross, Solid State Phenom. 128 (2007) 81.
[20] V. Sadykov, N. Mezentseva, V. Muzykantov, R. Bunina, A. Boronin, V. Voronin, I. Berger, Mater. Res. Soc. Symp. Proc. 1023 (2007), JJ02-07.1-6.
[21] V. Sadykov, N. Mezentseva, V. Muzykantov, E. Gubanova, N. Sazonova, A. Bobin, V. Voronin, J. Ross, C. Mirodatos, Mater. Res. Soc. Symp. Proc. 1122 (2009), O05-03.
[22] V.A. Sadykov, T.G. Kuznetsova, G.M. Alikina, Yu.V. Frolova, A.I. Lukashevich, V.S. Muzykantov, V.A. Rogov, L.G. Ivanov, S. Pinaeva, E. Neophytides, K. Kemnitz, C. Scheurel, Mirodatos, in: D.K. McReynolds (Ed.), New Topics in Catalysis Research, Nova Science Publishers, New York, 2007, pp. 97–196 (Chapter 5).
[23] T.G. Kuznetsova, V.A. Sadykov, S.A. Veniaminov, G.M. Alikina, E.M. Moroz, V.A. Rogov, O.N. Martyanov, V.F. Yudanov, I.S. Abornev, S. Neophytides, Catal. Today 91–92 (2004) 161.
[24] V. Sadykov, T.G. Kuznetsova, V.S. Muzykantov, L.G. Pinaeva, E.A. Paukshtis, N.V. Mezentseva, E. Kemnitz, C. Mirodatos, A.C. van Veen, Catal. Today 117 (2006) 475.
[25] V.S. Muzykantov, E. Kemnitz, V.A. Sadykov, V.V. Lunin, Kinet. Catal. 46 (2003) 319, doi:10.1023/A:1024486716938.
[26] F. Dong, A. Suda, T. Tanabe, Y. Nagai, H. Sobukawa, H. Shinjoh, M. Sugiura, C. Descorme, D. Duprez, Catal. Today 827 (2004) 93.
[27] N.N. Bulgakov, V.A. Sadykov, V.V. Lunin, E. Kemnitz, React. Kinet. Catal. Lett. (2002) 111.
[28] V.A. Sadykov, S.F. Tikhov, N.N. Bulgakov, A.P. Gerasev, Catal. Today 144 (2009) 324, doi:10.1016/j.cattod.2008.12.018.
[29] S.N Pavlova, N.N. Sazonova, V.A. Sadykov, G.M. Alikina, A.I. Lukashevich, E. Gubanova, R.V. Bunina, Stud. Surf. Sci. Catal. 167 (2007) 343.
[30] N.N. Sazonova, V.A. Sadykov, A.S. Bobin, S.A. Pokrovskaya, E.L. Gubanova, C. Mirodatos, React. Kinet. Catal. Lett. 98 (2009) 35.
[31] V. Vernikovskaya, L.N. Bobrova, L.G. Pinaeva, V.A. Sadykov, I.A. Zolotarskii, V.A. Sobyanin, I. Buyakou, V. Kalinin, S. Zhdanok, Chem. Eng. J. 134 (2007) 180.
[32] Yu. Ivanova, E. Sadovskaya, G. Pinaeva, V. Sadykov, C. Mirodatos, Chem. Sustain. Develop. 7 (2009) 371.
[33] D. Efremov, L. Pinaeva, V. Sadykov, C. Mirodatos, Solid State Ionics 179 (2008) 847.
[34] A.B. Mhadeshwar, D.G. Vlachos, Ind. Eng. Chem. Res. 46 (2007) 5310.
[35] G. Ertl, Adv. Catal. 37 (1990) 213.
[36] J. Zhu, J.G. van Ommen, L. Lefferts, J. Catal. 225 (2004) 388.
[37] Y. Liu, F.-Y. Huang, J.-M. Li, W.-Zh. Weng, Ch.-R. Luo, M.-L. Wang, W.-Sh. Xia, Ch.-J. Huang, H.-L. Wan, J. Catal. 256 (2008) 192.
[38] W.J. Stark, J.-D. Grunwaldt, M. Maciejewski, S.E. Pratsinis, A. Baiker, Chem. Mater. 17 (2005) 3352.
[39] J.-D. Grunwaldt, A. Baiker, Catal. Lett. 99 (2005) 5.
[40] S. Hannemann, J.-D. Grunwaldt, N. van Vegten, A. Baiker, P. Boye, Ch.G. Schroer, Catal. Today 126 (2007) 54.